PCCP

ROYAL SOCIETY OF CHEMISTRY

PAPER

View Article Online
View Journal | View Issue

Cite this: *Phys. Chem. Chem. Phys.*, 2026, **28**, 6743

Solubility and antisolvent crystallization of lithium hydroxide monohydrate in various organic solvents

Lien Lemmens,[a] Xavi Vanwezer,[a] Stijn Raiguel,[a] Rayco Lommelen,[a] Kerstin Forsberg,[b] Tom Van Gerven[c] and Koen Binnemans*[a]

Received 19th November 2025,
Accepted 18th February 2026

DOI: 10.1039/d5cp04491j

rsc.li/pccp

The effect of various organic antisolvents on the solubility of lithium hydroxide monohydrate ($LiOH{\cdot}H_2O$) in water was systematically determined in order to obtain composition data for lithium hydroxide – water – antisolvent ternary systems. Based on these data, antisolvent crystallization of $LiOH{\cdot}H_2O$ from a synthetic aqueous feed solution was investigated. A total of nine antisolvents were studied, including methanol, ethanol, acetone, 1-propanol, 2-propanol, 1,4-dioxane, 1,2-dimethoxyethane, acetonitrile and tetrahydrofuran (THF). $LiOH{\cdot}H_2O$ showed high solubility in methanol and ethanol, and low solubility in 2-propanol, 1,4-dioxane and 1,2-dimethoxyethane aqueous solutions. The use of THF resulted in the formation of two liquid phases in all cases, while acetonitrile and 1-propanol also led to liquid phase separation at lower antisolvent mole fractions. In the acetone system, solvent decomposition was confirmed by ^{1}H NMR, revealing aldol condensation. Crystallization of $LiOH{\cdot}H_2O$ was confirmed for all antisolvents by X-ray diffraction (XRD) and thermogravimetric analysis (TGA). Among the tested solvents, 2-propanol was selected as the most promising antisolvent due to its favorable solubility behavior, environmental and human health profile, safety, and lower cost compared to 1,4-dioxane and 1,2-dimethoxyethane.

Introduction

Lithium hydroxide monohydrate ($LiOH{\cdot}H_2O$) is a critical component in the synthesis of nickel-rich NMC (nickel–manganese–cobalt) cathode active materials (CAMs). As the CAM becomes richer in nickel, $LiOH{\cdot}H_2O$ is preferred over lithium carbonate (Li_2CO_3) in the production process for several reasons. When Li_2CO_3 is used for the synthesis of these nickel-rich NMC CAMs, higher temperatures are required to complete the synthesis, which can damage the crystal structure of the cathode. In contrast, $LiOH{\cdot}H_2O$ enables faster and more efficient synthesis at lower temperatures, preserving the structural integrity and performance of the cathode.[1–3] However, the challenge of working with $LiOH{\cdot}H_2O$ is that it can react with CO_2, which results in the undesirable formation of Li_2CO_3.[4] This reactivity necessitates careful handling and controlled processing environments to maintain product quality and efficacy. Even trace amounts of Li_2CO_3 impurities do not decompose and instead remain trapped in the cathode, causing lithium deficiency and structural instability.[5]

High-purity $LiOH{\cdot}H_2O$ is typically produced through hydrometallurgical processes, either from primary sources like spodumene or from secondary sources like used lithium-ion batteries. These processes generally include pretreatment, leaching, separation, purification, conversion and finally crystallization.[6–8] The crystallization process should be designed to produce crystals of desired quality in terms of purity, size, and size-distrubution.[9]

The conventional method for crystallizing $LiOH{\cdot}H_2O$ is evaporative crystallization, which involves heating the solvent to reduce its volume by evaporation, driving crystallization.[10] However, this method is associated with high energy consumption.[9] Cooling crystallization, relies on cooling of the solvent to reduce the solubility of the solute. This method is less suitable for $LiOH{\cdot}H_2O$, because $LiOH{\cdot}H_2O$ has a small variation in solubility with temperature, limiting the maximum yield of the process.[11] Given the limitations of conventional methods, *antisolvent crystallization* (also known as *drowning-out crystallization*) received more attention. This method involves the addition of a second miscible liquid, known as the *antisolvent*, in which the compound to be crystallized has no or very low solubility. The introduction of the antisolvent reduces the overall solubility of the compound in the mixture, creating supersaturation and promoting crystallization.[10] Antisolvent

[a] *KU Leuven, Department of Chemistry, Celestijnenlaan 200F, Box 2404, B-3001 Leuven, Belgium. E-mail: Koen.Binnemans@kuleuven.be*
[b] *KTH Royal Institute of Technology, Department of Chemical Engineering, Stockholm, Sweden*
[c] *KU Leuven, Department of Chemical Engineering, Celestijnenlaan 200F, Box 2424, B-3001 Leuven, Belgium*

crystallization offers better control over supersaturation compared to evaporative crystallization, as various parameters can be controlled, including the selection of the antisolvent, its addition rate, and the concentration of the antisolvent. All these parameters will have an influence on the crystal size, morphology, yield and the hydration state (LiOH or $LiOH{\cdot}H_2O$) of the crystals, which are important in CAM production.[9,12] Despite these advantages, studies on $LiOH{\cdot}H_2O$ crystallization *via* antisolvents remain limited, with ethanol being one of the few systems previously explored.[13,14]

One such study is that of Graber *et al.*,[14] who compared $LiOH{\cdot}H_2O$ crystals obtained by simple evaporation with those precipitated by ethanol addition. They reported differences in XRD patterns, which they interpreted as indicative of polymorphic behavior. However, unlike other alkali hydroxides, LiOH exhibits no known polymorphism under ambient conditions.[15] The claims of additional polymorphs have not been independently verified, and later authors have raised methodological concerns about aspects of Graber's analysis.[16] The reported differences are more plausibly attributed to variations in preferred orientation, minor Li_2CO_3 contamination, partial dehydration, or solvate inclusion, rather than a distinct polymorphic phase.[17]

In order to be effective, the antisolvents should ideally meet several criteria. First, the antisolvents should be miscible with aqueous solutions to ensure homogeneous mixing and facilitate efficient solubility reduction. A low dielectric constant is also desirable since this facilitates ion pairing, which is essential for reducing the solubility of $LiOH{\cdot}H_2O$ in the solution. In addition, antisolvents that are environmentally friendly and inexpensive are preferred to support both sustainability and economic feasibility. A relatively low boiling point is also advantageous, as it allows recovery by distillation at moderate temperatures. In addition, the boiling point should ideally differ sufficiently from that of water to ensure effective separation during distillation. Furthermore, chemical stability is important to prevent undesirable side reactions that could affect purity. By meeting as many of these criteria as possible, antisolvents can optimize the crystallization process, improving both the efficiency and sustainability of $LiOH{\cdot}H_2O$ production.[9,18–20]

A key factor in developing any crystallization process is understanding the solubility behavior of the solute. Accurate solubility data are essential not only for solvent and antisolvent screening, but also for process design, scale-up, and operation. Unfortunately, such data are often unavailable, particularly for ternary and mixed solvent systems, non-aqueous solvents, or solutions containing impurities. These are conditions that more closely represent real industrial processes. Predictive thermodynamic models can assist in initial screening, but their reliability is often limited due to incomplete or unavailable thermodynamic and equilibrium data. As a result, experimental determination of solubility remains the most reliable approach for generating the necessary data for process development.[10]

In this work, the effect of various organic antisolvents on the solubility of $LiOH{\cdot}H_2O$ in water was experimentally determined to support the design and evaluation of an antisolvent crystallization route. Ternary phase behavior was mapped to assess crystallization potential, and the performance of each antisolvent was evaluated based on solubility behavior, miscibility, chemical compatibility, environmental impact, and recovery feasibility. This research aims to provide a more sustainable and controllable pathway for producing battery-grade $LiOH{\cdot}H_2O$, and to address the knowledge gap in solubility data for this system.

Experimental

Chemicals

Lithium hydroxide monohydrate ($\geq$98%), methanol ($\geq$99.8%), 2,6-pyridinedicarboxylic acid (99%), sodium tartrate dihydrate and 2-propanol ($\geq$99.8%) were obtained from Merck KGaA (Darmstadt, Germany). Buffer solutions of pH 1.00, pH 4.00, pH 7.00, pH 12.00, heptane ($\geq$99%), acetonitrile ($\geq$99.5%) and 1000 mg L^{-1} standard solution of lithium (in H_2O) were purchased from Chem-Lab (Zedelgem, Belgium). Nitric acid concentrate 0.1 mol L^{-1} HNO_3 in water (for IC) and tetrahydrofuran ($\geq$99.8%) were purchased from Sigma-Aldrich (Steinheim, Germany). Hydranal™ composite 5 and hydranal™ methanol dry were obtained from Fluka (Seelze, Germany). Tris-(hydroxymethyl)-aminomethane was purchased from VWR (Leuven, Belgium). Acetone ($\geq$99.8%), 1-propanol (99.5%) and ethanol (99.8%) were purchased from Fisher Scientific (Loughborough, United Kingdom). Ethylene glycol dimethyl ether ($\geq$99%) and 1,4-dioxane ($\geq$99.5%) were obtained from Acros Organics (Geel, Belgium). Hydrochloric acid 0.1 mol L^{-1} was purchased from Th. Geyer (Renningen, Germany). Ultrapure water with a resistivity of 18.2 MΩ cm was produced using a Milli-Q® Reference Water Purification System from Merck Millipore. All products were utilized in their original state without any further purification.

Instrumentation

Ion chromatography (IC) was used for the analysis of lithium in the solutions. The analyses were carried out using a Shimadzu IC setup with a CBM-40 system controller, DGU-403 degassing unit, LC-20Ai pump, SIL20A autosampler, CTO-40C column oven and a CDD-10A vp conductivity detector. A Metrohm Metrosep C4 column was used and the injection volume was 10 μL. Calibration was performed using an external standard series containing 1, 5, 10, 50 and 100 mg L^{-1} lithium. The samples were properly diluted in ultrapure water to ensure that their concentrations fell within the range of the calibration. The eluent used for IC was composed of 0.7 mmol L^{-1} pyridine-2,6-dicarboxylic acid and 1.7 mmol L^{-1} nitric acid in ultrapure water. The pump flow rate of the eluent was set at 0.9 mL min^{-1} and the oven temperature was maintained at 25 °C during the analyses.

Density measurements of the solutions were performed using an Anton Paar DMA 4500 M oscillating U-tube. The measurements were carried out at 25 °C.

The water content in the solutions at equilibrium was determined by Karl Fischer titration using a Mettler Toledo V30S volumetric titrator. Sodium tartrate dihydrate was used as the volumetric standard for titer determination. Since the hydroxide ions in the solutions were protonated by the buffer in the titration vessel and thus quantitatively converted to water during the Karl Fischer measurements, the hydroxide concentration (equal to the lithium concentration determined by IC) was subtracted from the apparent water content measured by Karl Fischer titration.

Thermogravimetric analysis (TGA) was used to quantitatively determine the hydration state of the precipitated LiOH. These analyses were performed with a TA Instruments TGA-Q500, using a heating rate of 10 °C min^{-1} from 20 °C up to 150 °C on samples between 7 and 15 mg.

The obtained crystals were characterized by a powder X-ray diffraction (XRD) analysis, performed on a Bruker D2 phaser Diffractometer with Cu-Kα radiation (30 kV, 10 mA, step size of 0.08°, a counting of 0.25 s per step in the measurement range 2θ of 5 to 100°). Data processing was executed with the Bruker DIFFRAC.EVA software.

Acid–base titration was performed to ensure that no significant quantity of Li_2CO_3 was formed. For this, the crystals were first brought in solution by adding 0.02 g of the crystals to 2 mL of ultrapure water. Subsequently, the mixture was stirred for at least 1 hour under argon atmosphere. The hydroxide and carbonate concentrations were measured by an automated titration, utilizing an automated titrator (Mettler Toledo T5 Excellence), equipped with a combined glass pH electrode (Mettler Toledo DMi111-SC) and an InMotion Autosamples Flex autosampler. Ultrapure water was used to rinse the pH electrode. The calibration of the titrant (0.1 mol L^{-1}) was performed by adding 40 mL of ultrapure water to approximately 60 mg of dry tris-(hydroxymethyl)-aminomethane in a titration beaker. During the analyses, the solutions were kept under inert (argon) atmosphere by connecting a balloon filled with argon to the samples to prevent formation of Li_2CO_3 while running the measurements. Based on the titration setup, the method allows detection of Li_2CO_3 down to approximately 0.2 wt% in the crystal sample.

High-field nuclear magnetic resonance (NMR) spectra were recorded on a Bruker Avance III HD 400 spectrometer with a Bruker Ascend™ 400 magnet system (^{1}H basic frequency of 400.17 MHz) and a 5 mm PABBO BB/19F-1H/D probe with z-gradients. All samples were dissolved in DMSO-d_6. Data were recorded at room temperature using Bruker TopSpin 3 and processed and analyzed using Spinworks 4.2.12. ^{1}H data were calibrated using tetramethylsilane (TMS) as an internal calibration reference. The δ-values are expressed in parts per million (ppm).

Solubility experiments

To determine the solubility of $LiOH{\cdot}H_2O$ in different water–antisolvent mixtures, both the precipitation method and the isothermal dissolution method were used.

For the preparation of saturated aqueous $LiOH{\cdot}H_2O$ solutions, an excess of solid $LiOH{\cdot}H_2O$ was added to a certain amount of ultrapure water under an argon atmosphere. The glass reagent bottle was immersed in a temperature-controlled water bath at 25 °C and magnetically stirred at 400 rpm. The time to reach dissolution equilibrium was determined by taking samples as a function of time under these experimental conditions. Based on the results, a minimum of 24 hours equilibration time was chosen. At the end of the experiment, when equilibrium was established, stirring was stopped and the solution was filtered over a 1.6 μm pore size filter to remove the larger particles. The supernatant was centrifuged and filtered through a 0.22 μm syringe filter. The lithium concentration was then measured by IC, the density was determined at 25 °C, and the water content was measured by Karl Fischer titration. In this work, lithium concentrations correspond to the mass of elemental Li determined *via* Li^+ detection by ion chromatography and are reported as g Li per kg H_2O.

In the precipitation method, a known quantity of antisolvent was added to the saturated solution of LiOH in water to obtain a specific organic-over-aqueous (O/A) mass ratio. The antisolvent was added last and quickly to avoid losses through evaporation. The mixture was then stirred at 25 °C and 400 rpm for 24 hours. Then, the suspension was filtered using a Büchner funnel to separate the supernatant and the solid phase. The supernatant was centrifuged and filtered by using 0.22 μm syringe filters. The lithium concentration was determined by IC analysis and the density was measured at 25 °C. Because $LiOH{\cdot}H_2O$ crystallizes with one bound water molecule, the water content at equilibrium differs from the initial composition. Therefore, Karl Fischer titration was used to determine the actual water content of the equilibrated solution. The solid phase after filtration was subjected to TGA analysis to quantify the level of hydration in the solid. XRD analysis and acid–base titration were employed to confirm the phase composition of the precipitate and to verify that no significant amount of Li_2CO_3 had formed.

In the isothermal dissolution method, an excess of solid $LiOH{\cdot}H_2O$ was added directly to a water–antisolvent mixture with a predefined O/A mass ratio. The time to reach equilibrium was determined by taking samples as a function of time. Based on the results, a minimum of 24 hours equilibration time was chosen. The mixture was then stirred at 25 °C and 400 rpm for 24 hours. After stirring the mixture for 24 hours, the same analytical techniques, *i.e.* IC, density measurement, Karl Fischer titration, TGA, XRD and acid–base titration, were applied to characterize each phase. Wherever possible, the procedures were carried out under an argon atmosphere to minimize contact with atmospheric CO_2 and hence to prevent the formation of Li_2CO_3.

Lithium solubility calculation and water content correction

The lithium solubility data are expressed in units of g Li per kg H_2O (g kg^{-1} H_2O), a common unit in solubility studies to allow comparison between aqueous systems of varying water content. The concentration of lithium in solution was determined by IC

and obtained in g L^{-1}. In this work, ''lithium concentration'' refers to the mass of elemental lithium measured *via* Li^+ detection by ion chromatography and expressed as g Li per kg H_2O. This value does not represent metallic lithium or the concentration of lithium salts. To convert the lithium concentration from g L^{-1} to g Li kg^{-1} H_2O, the following expression was used:

$$\text{Li solubility}\left(\text{g kg}^{-1}\,\text{H}_2\text{O}\right) = \frac{C_{\text{Li}}\left(\text{g L}^{-1}\right)}{\rho\left(\text{kg L}^{-1}\right)} \times \frac{1}{\omega_{\text{H}_2\text{O,real}}} \quad (1)$$

here, C_{Li} is the lithium concentration (g L^{-1}), ρ is the solution density (kg L^{-1}), and $\omega_{H_2O,real}$ is the real mass fraction of water in the solution.

The real water mass fraction, $\omega_{H_2O,real}$, was determined by Karl Fischer titration and corrected for the presence of hydroxide ions *(vide supra)*. This correction is necessary because hydroxide reacts with the Karl Fischer reagent and would otherwise falsely contribute to the measured water content. Therefore, the true water content was calculated as:

$$\omega_{\text{H}_2\text{O,real}} = \omega_{\text{KF,measured}} - \omega_{\text{OH}^-} \quad (2)$$

here, $\omega_{KF,measured}$ is the mass fraction of water as measured by Karl Fischer titration, and ω_{OH^-} is the mass fraction of hydroxide ions (as LiOH), calculated from the measured lithium concentration assuming a 1 : 1 molar ratio between Li^+ and OH^-.

This correct mass fraction ensures that only the actual water content is used in the calculation of lithium solubility.

Conversion to mole fractions

To facilitate comparison across antisolvents, the solubility results are expressed in terms of mole fraction of antisolvent at equilibrium, rather than O/A mass ratios. This approach provides a more meaningful basis for comparison, as it accounts for differences in molecular mass between antisolvents. The mole fraction of antisolvent at equilibrium, $\chi_{antisolvent}$, was calculated as:

$$\chi_{\text{antisolvent}} = \frac{n_{\text{antisolvent}}}{n_{\text{LiOH}} + n_{\text{water}} + n_{\text{antisolvent}}} \quad (3)$$

Results and discussion

Equilibration time in pure water

The time needed to reach the solid–liquid equilibrium in solubility experiments can vary from several hours to a few days depending on the solute and the conditions used.[21] According to the handbook of industrial crystallization, the solution should be stirred for a minimum of 4 hours, although a 24-hour stirring period is preferred.[10] Taboada *et al.*[11] reported a stirring time of 48 hours to reach the equilibrium of lithium hydroxide (LiOH) in pure water. Fig. 1 shows the lithium concentration as a function of time, measured using the isothermal dissolution method. Each data point represents the average of three replicate measurements, and the error bars indicate the standard error of the mean. Samples were taken after 1 h, 3 h, 5 h, 24 h, 48 h and 1 week. The results indicate that the solid–liquid equilibrium is reached very rapidly.

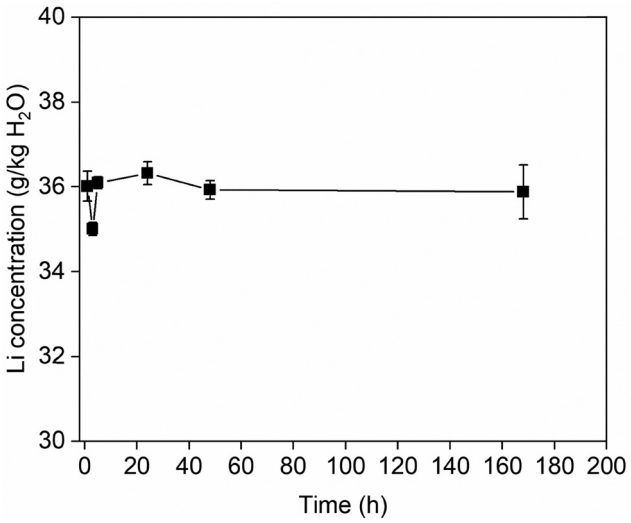

Fig. 1 Lithium concentration (g kg^{-1} H_2O) as a function of time in pure water at 25 °C.

Therefore, an equilibration time of 24 hours was used further in this study. The measured solubility of LiOH in pure water at 25 °C in this research was 10.95 ± 0.06 wt%. This result aligns well with values reported in the literature, which include 11.00 wt% (Kirk-Othmer),[11] 11.14 wt% (Linke and Seidell),[22] 11.03 wt% (Taboada *et al.*),[11] 11.34 wt% (international critical tables)[11] and 11.10 wt% (CRC handbook of chemistry and physics).[23] Expressed in terms of grams of LiOH per 100 g of water, the solubility determined in this study corresponds to 12.53 ± 0.09 g/100 g H_2O. This is in close agreement with the value reported in the CRC Handbook of Chemistry and Physics, which is 12.5 g/100 g H_2O.[23]

Analyses of the solid phase confirmed the presence of LiOH·H_2O. Fig. 2 presents the TGA curve, showing the percentage mass loss as a function of temperature. The theoretical percentage of mass loss due to the release of crystal water from LiOH·H_2O is 42.92%. The experimentally determined mass loss was

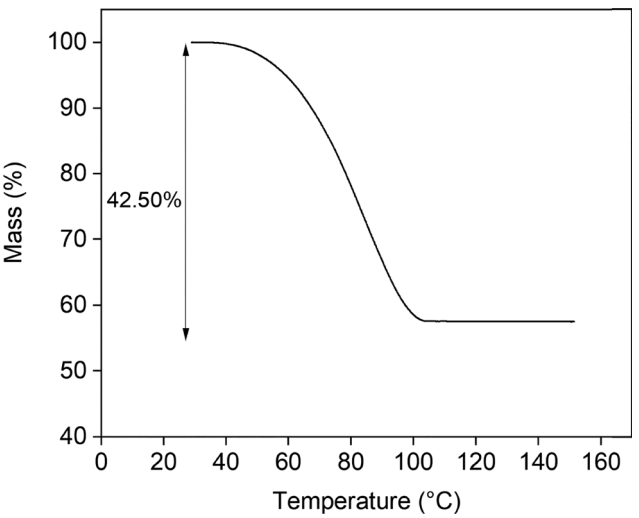

Fig. 2 TGA curve showing mass loss *versus* temperature.

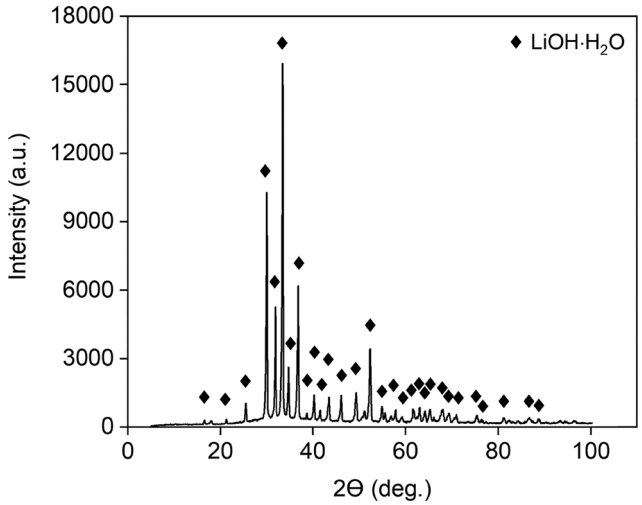

Fig. 3 XRD diffractogram confirming the presence of $LiOH{\cdot}H_2O$.

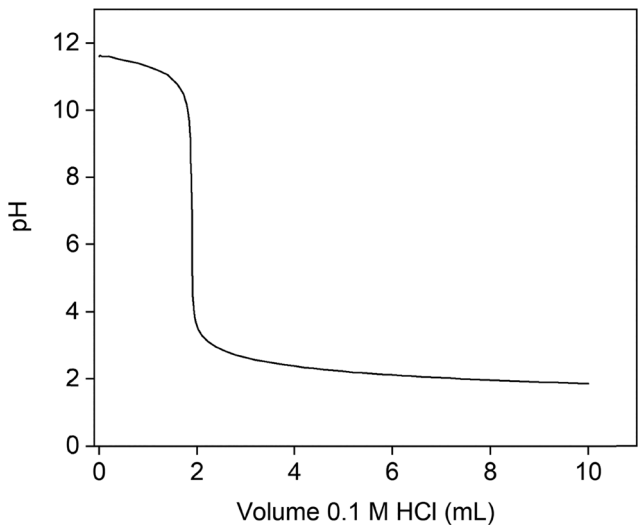

Fig. 4 Titration curve with a single equivalence point.

42.50%, which is in close agreement with the theoretical value, further supporting the presence of $LiOH{\cdot}H_2O$.

To confirm this result, XRD analysis was performed (Fig. 3). The XRD diffractogram confirms the presence of $LiOH{\cdot}H_2O$ and indicates that no significant amounts of anhydrous LiOH or Li_2CO_3 were present. To verify the absence of Li_2CO_3, an acid–base titration was carried out (Fig. 4). The titration curve shows a single equivalence point, indicating that no significant amount of Li_2CO_3 had formed.

Equilibration time in water–antisolvent systems

Nine antisolvents were investigated in this research: methanol, ethanol, acetone, 1-propanol, 2-propanol (isopropanol), 1,4-dioxane, 1,2-dimethoxyethane, acetonitrile and tetrahydrofuran (THF). These antisolvents were selected based on the criteria outlined in the introduction, including miscibility with water,

Table 1 Boiling points, dielectric constants, specific heat capacities, and enthalpies of vaporization of the investigated antisolvents

Antisolvent	Boiling point (°C)[25]	Dielectric constant (ε, 20 °C)[26]	Specific heat capacity ($J\ g^{-1}\ K^{-1}$) at 25 °C)[23]	Enthalpy of vaporization (T_b) ($J\ g^{-1}$)[23]
Water	100	80.10	4.180	2256.2
Methanol	65	33.00	2.531	1098.5
Ethanol	78	25.30	2.438	836.9
Acetone	56	21.01	2.175	501.3
1-Propanol	97	20.80	2.395	689.8
2-Propanol	82	20.18	2.604	663.5
1,4-Dioxane	102	2.22	1.726	387.7
1,2-Dimethoxyethane	85	7.30[a]	2.145	360.0
Acetonitrile	82	36.64	2.229	724.9
THF	65	7.52[b]	1.720	413.5

[a] Dielectric constant at 24 °C. [b] Dielectric constant at 22 °C.

relatively low dielectric constant, cost, and a sufficiently low boiling point to enable recovery by distillation. For comparison, the boiling points, dielectric constants, specific heat capacities, and enthalpies of vaporization of these antisolvents are summarized in Table 1. The inclusion of specific heat capacity and enthalpy of vaporization allows an estimation of the energy required for antisolvent recovery *via* distillation. The specific heat capacity indicates the amount of energy needed to heat the liquid to its boiling point, while the enthalpy of vaporization represents the energy required for the phase transition from liquid to vapor. By considering both parameters, the relative energy demand for distillation of the different antisolvents can be assessed. For instance, antisolvents with a lower specific heat capacity require less energy to reach their boiling point, and those with a lower enthalpy of vaporization require less energy for the actual vaporization step. Therefore, both properties directly influence the overall energy consumption during recovery.[24]

The total theoretical energy required for solvent recovery by distillation was estimated according to eqn (4).

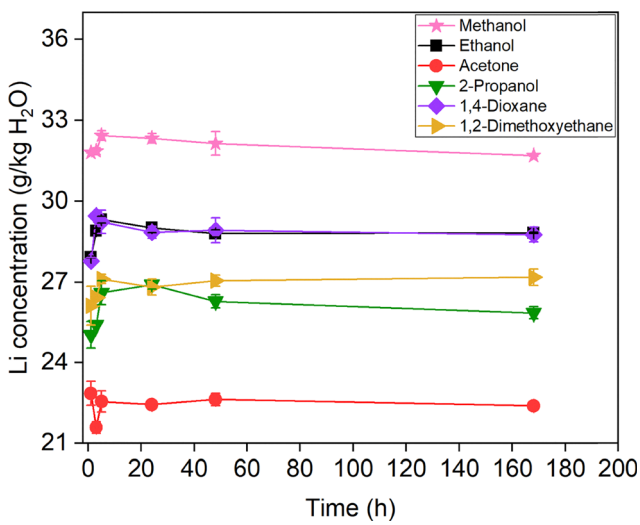

Fig. 5 Variation of the lithium concentration as a function of time at 25 °C using the isothermal dissolution method with a 1/10 O/A ratio. Results are shown only for systems where a single liquid phase was observed.

$$Q_{Total} = c_p(T_b - T_0) + \Delta H_{vap} \quad (4)$$

In this equation is c_p the specific heat capacity of the liquid (J g^{-1} K^{-1}), T_b is the boiling point (°C), T_0 is the initial temperature (25 °C), and ΔH_{vap} is the enthalpy of vaporization of the liquid (J g^{-1}). The c_p values at 25 °C were used as constant approximations, since their temperature dependence has a minor influence compared to the vaporization enthalpy.

Six different O/A ratios based on mass were tested, with the organic component acting as the antisolvent. The O/A ratios investigated in this study were 1/10, 1/4, 1/1, 2/1, 4/1, and 6/1. To determine the required equilibration time, time-dependent concentration measurements were carried out for the two extreme ratios: the one with the lowest antisolvent content (1/10) and the one with the highest (6/1). These experiments were conducted using the isothermal dissolution method. The lithium concentration for the 1/10 O/A ratio as a function of time at 25 °C is shown in in Fig. 5. The results indicated that equilibrium was reached rapidly.

When 1-propanol, acetonitrile and THF were used as antisolvents, two liquid phases were observed. Therefore, these results are not shown in the figure. In the case of acetone, a noticeable color change suggested that a chemical reaction occurred (*vide infra*).

Analyses of the solid phases confirmed the presence of LiOH·H_2O. The TGA curves (Fig. S1 in SI) show the percentage mass loss as a function of temperature for all antisolvent systems. The experimentally determined mass losses closely matched the theoretical value for the loss of water of hydration, supporting the conclusion that LiOH·H_2O was present in all cases. The XRD diffractograms (Fig. S2 in SI) further confirmed the presence of LiOH·H_2O and indicated that no significant amounts of anhydrous LiOH or Li_2CO_3 had formed. The acid–base titration curves (Fig. S3 in SI) for the crystals obtained with each antisolvent showed a single equivalence point, consistent with the absence of significant Li_2CO_3 formation.

The solubility of lithium as a function of time for the 6/1 O/A ratio at 25 °C is shown in Fig. 6. The results indicated again that solid–liquid equilibrium was reached rapidly, within approximately 5 hours. In this case, the use of 1-propanol and acetonitrile no longer resulted in the formation of two liquid phases. However, when THF was used, liquid phase separation was still observed. That is why the data of THF are not included in the figure. As previously noted, the use of acetone caused a visible color change, again suggesting that a chemical reaction occurs. Results for methanol are also not shown, as the measured concentration (in g kg^{-1} H_2O) exceeded that of LiOH in pure water. This apparent increase can be explained by the relatively high intrinsic solubility of LiOH·H_2O in methanol. When the concentration is expressed per mass of water, the calculated solubility appears to be higher. At higher methanol mole fractions, the large volume of added solvent dilutes the overall LiOH·H_2O content of the mixture below its saturation limit for the given composition. Consequently, crystallization does not occur, despite the lower solubility of LiOH·H_2O in pure methanol. Based on the rapid attainment of equilibrium

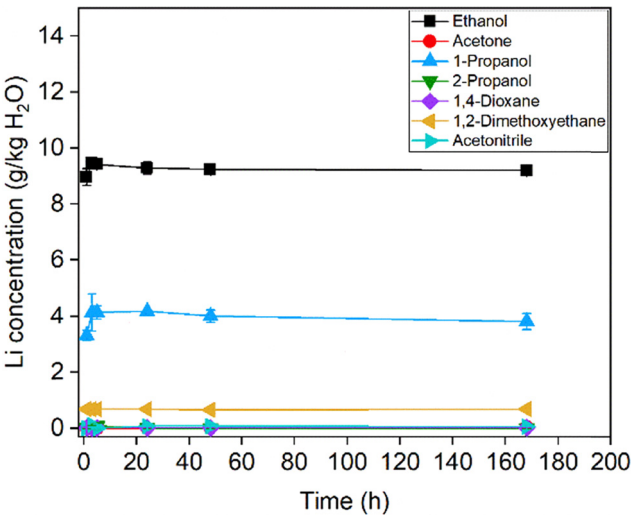

Fig. 6 Variation of the lithium concentration as a function of time at 25 °C using the isothermal dissolution method with a 6/1 O/A ratio.

observed, a duration of 24 hours was selected for subsequent experiments to ensure that equilibrium was fully established under all tested conditions.

The TGA curves (Fig. S4 in SI) demonstrated that the experimentally determined mass losses closely matched the theoretical value for the loss of water of hydration, confirming the presence of LiOH·H_2O in all samples. The XRD diffractograms (Fig. S5 in SI) further indicated the presence of LiOH·H_2O and showed no significant evidence for presence of anhydrous LiOH or Li_2CO_3. Finally, the acid–base titration curves (Fig. S6 in SI) for all crystals showed that no significant amount of Li_2CO_3 had formed.

Solubility of LiOH·H_2O in different water–antisolvent mixtures

All listed O/A ratios were tested with each of the nine antisolvents, using the precipitation method. This method was chosen for its practical advantage in visualizing crystallization. For example, in the case of methanol at a 6/1 ratio, no crystallization occurred when starting from a saturated solution due to excessive dilution. Such cases would not be captured effectively using the dissolution method. Although the dissolution method is generally considered more reliable, since it avoids the formation of metastable intermediate phases often encountered in precipitation, it was important to analyze the solid phases in all cases to verify the results.[21]

Because it is practically difficult to weigh exactly the same mass for each sample (*e.g.*, 7.0109 g *vs.* 7.0318 g), slight variations in the O/A ratio occur. Therefore, each data point is shown individually (Fig. 7) with its corresponding mole fraction of antisolvent, rather than as an average. For clarity, the lithium concentrations in LiOH–water–solvent mixtures at 25 °C are also presented separately for each antisolvent in Fig. S7–S14 in the SI. In addition, the 24-hour time-dependent solubility data obtained *via* the isothermal dissolution method (*vide supra*) are included in the figure as open symbols to clearly illustrate method validation. These data fit well with the trend

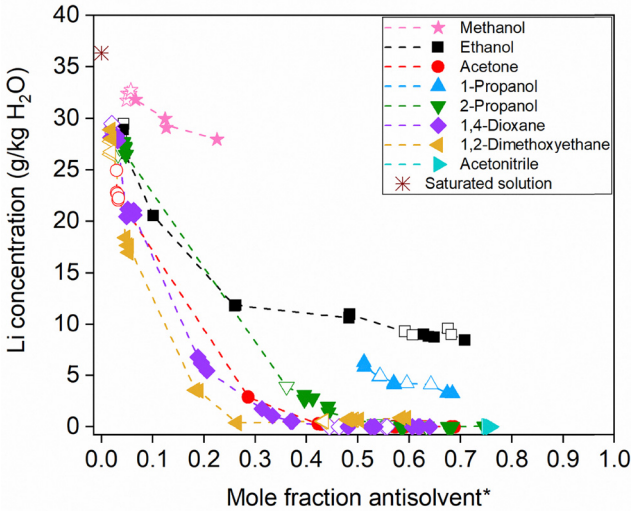

Fig. 7 Lithium concentration in LiOH–water–solvent mixtures at 25 °C. Open symbols: isothermal dissolution method; closed symbols: precipitation method. *Mole fraction of antisolvent at equilibrium.

observed from the precipitation results, confirming consistency between the two approaches and indicating that metastable supersaturated solutions did not form in the precipitation method. Immediate crystallization observed upon antisolvent addition in the precipitation method suggests that the system reaches solid–liquid equilibrium very fast.

As shown in Fig. 7, LiOH·H_2O exhibits a high solubility in methanol, making methanol unsuitable as an antisolvent since it does not sufficiently reduce the solubility of LiOH·H_2O. Even at higher mole fractions of methanol, no crystallization was observed, and therefore, no solubility values could be determined in this region. LiOH·H_2O also shows high solubility in ethanol and 1-propanol. In the case of 1-propanol, two liquid phases were observed at lower mole fractions, which hindered accurate solubility determination under these conditions. For 2-propanol, a liquid–liquid phase separation was observed at the 1/1 O/A mass ratio. At higher 2-propanol fractions the mixture again formed a single homogeneous liquid, consistent with observations for alkaline 2-propanol–water systems containing LiOH.[27] This does not affect applicability, since process-relevant antisolvent crystallization and solvent recovery operate at higher 2-propanol fractions than 1/1. In contrast, the water–acetone mixture resulted in a very low solubility of LiOH·H_2O. However, a visible color change suggested a chemical reaction involving the solvent, complicating interpretation of the results. THF remained immiscible with the aqueous phase at all investigated antisolvent mole fractions. Acetonitrile led to the formation of two liquid phases in most cases, except at high mole fractions of acetonitrile, which limited its applicability. The measured compositions of the coexisting liquid phases, together with their densities and water contents, are reported for acetonitrile in Table S1 in SI.

Both 1,2-dimethoxyethane and 1,4-dioxane significantly reduced the solubility of LiOH·H_2O and were miscible with water, but their use is limited by concerns regarding sustainability and potential health risks.[25] Among the tested solvents, 2-propanol appears to be a promising candidate for antisolvent crystallization. It effectively reduces the solubility of LiOH·H_2O, is miscible with water over the process-relevant composition range, and does not show evidence of reactivity with the solute. In addition to its favorable solubility behavior, 2-propanol offers advantages in terms of process efficiency, cost, environmental impact, and safety.[25] Notably, its lower boiling point (82 °C) compared to that of 1,4-dioxane (102 °C) and 1,2-dimethoxyethane (85 °C) (Table 1) is advantageous for antisolvent recovery, as it provides a larger temperature difference relative to water, facilitating separation during distillation.[24,25] While the total theoretical energy required for distillation (Q_{total}) per gram of solvent, calculated according to eqn (4) using the values in Table 1, is higher for 2-propanol ($\approx$811.9 J g^{-1}) than for 1,4-dioxane ($\approx$520.6 J g^{-1}) and 1,2-dimethoxyethane ($\approx$488.7 J g^{-1}),

Table 2 Lithium concentration at equilibrium as a function of antisolvent mole fraction for various antisolvents

Methanol		Ethanol		Acetone		1-Propanol	
Mole fraction antisolvent at eq.	Li concentration (g kg^{-1} H_2O)	Mole fraction antisolvent at eq.	Li concentration (g kg^{-1} H_2O)	Mole fraction antisolvent at eq.	Li concentration (g kg^{-1} H_2O)	Mole fraction antisolvent at eq.	Li concentration (g kg^{-1} H_2O)
0.05	3.209×10^{1}	0.10	2.054×10^{1}	0.03	2.294×10^{1}	0.51	6.033
0.13	2.937×10^{1}	0.26	1.182×10^{1}	0.29	2.889	0.57	4.180
0.22	2.795×10^{1}	0.48	1.080×10^{1}	0.43	2.556×10^{-1}	0.68	3.256
		0.64	8.783	0.53	4.521×10^{-3}		
		0.71	8.436	0.68	1.659×10^{-3}		

2-Propanol		1,4-Dioxane		1,2-Dimethoxyethane		Acetonitrile	
Mole fraction antisolvent at eq.	Li concentration (g kg^{-1} H_2O)	Mole fraction antisolvent at eq.	Li concentration (g kg^{-1} H_2O)	Mole fraction antisolvent at eq.	Li concentration (g kg^{-1} H_2O)	Mole fraction antisolvent at eq.	Li concentration (g kg^{-1} H_2O)
0.05	2.701×10^{1}	0.05	2.082×10^{1}	0.05	1.766×10^{1}	0.76	1.206×10^{-4}
0.40	2.873	0.20	5.793	0.19	3.536		
0.44	1.666	0.37	5.386×10^{-1}	0.26	3.780×10^{-1}		
0.59	5.349×10^{-3}	0.48	1.475×10^{-2}	0.43	5.354×10^{-1}		
0.68	5.182×10^{-4}	0.62	6.026×10^{-3}	0.50	6.695×10^{-1}		

this difference becomes smaller when expressed per mole of solvent (≈48.8, 45.9, and 44.0 kJ mol^{-1}, respectively). Despite the slightly higher Q_{total}, 2-propanol remains the preferred antisolvent due to its favorable combination of solubility behavior, water miscibility, environmental and safety profile, and the ability to form an azeotrope with water at a higher antisolvent mole fraction (~68 mol%) compared to 1,4-dioxane (~48 mol%) and 1,2-dimethoxyethane (~64 mol%).[28] This azeotrope characteristic supports more efficient solvent recovery and reuse, as it allows for the distillation of a less water-diluted azeotrope, resulting in a higher concentration of antisolvent in the recovered phase.

As shown in Table 2, the addition of each tested antisolvent, as well as increasing its concentration, leads to a decrease in lithium solubility. Polar protic solvents such as methanol, ethanol, 1-propanol, and 2-propanol are capable of solvating both lithium cations and hydroxide anions *via* ion-dipole interactions and hydrogen bonding, resulting in higher $LiOH{\cdot}H_2O$ solubility.[9] However, $LiOH{\cdot}H_2O$ solubility decreases in the order: methanol > ethanol > 1-propanol > 2-propanol, correlating with increasing alkyl-chain length. As the alkyl chains become longer, the dielectric constant of the solvents decreases, promoting ion association and thus reducing solubility.[20,29] Notably, the solubility in 2-propanol is comparatively lower than in 1-propanol, likely due to steric hindrance around the hydroxyl group, which reduces the lithium cation coordination efficiency.

In contrast, the polar aprotic solvents acetone, 1,4-dioxane, 1,2-dimethoxyethane, THF, and acetonitrile, can solvate lithium cations, but cannot effectively stabilize hydroxide anions due to the absence of hydrogen bond donating groups. This results in a lower solubility of $LiOH{\cdot}H_2O$.[9] 1,2-Dimethoxyethane can chelate lithium ions, resulting in a relatively high lithium solubility compared to other solvents with a similar dielectric constant. 1,4-Dioxane also possesses two coordinating ether moieties, but its rigid cyclic structure limits its chelation ability. Acetonitrile, with a moderately donating nitrogen lone pair and the lowest *Gutmann Donor Number* (DN) among the solvents studied (DN = 14.1 kcal mol^{-1}), exhibits weaker cation coordination. In contrast, oxygen-based solvents such as acetone (DN = 17.0 kcal mol^{-1}), 1,4-dioxane (DN = 14.8 kcal mol^{-1}), 1,2-dimethoxyethane (DN = 20 kcal mol^{-1}), and THF (DN = 20.0 kcal mol^{-1}) possess higher donor numbers, consistent with their stronger Li^+ coordination and the observed differences in $LiOH{\cdot}H_2O$ solubility.[30]

However, the solubility of lithium does not follow a straightforward or consistent trend when plotted against the dielectric constant of the solution, which is calculated using eqn (5). This equation takes into account the dielectric constants, molecular masses, and mole fractions of the individual solvents in the mixture, where x_i is the mole fraction, M_i is the molecular mass,

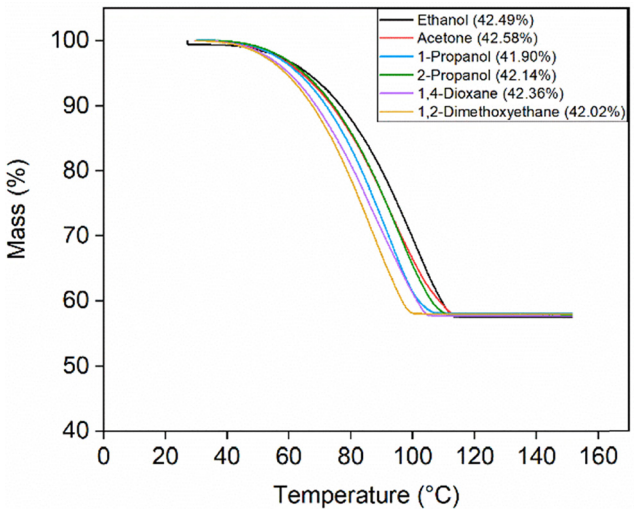

Fig. 9 TGA curves showing the percentage mass loss as a function of temperature for the solid phases obtained from solubility experiments using different antisolvents at an O/A ratio of 2/1.

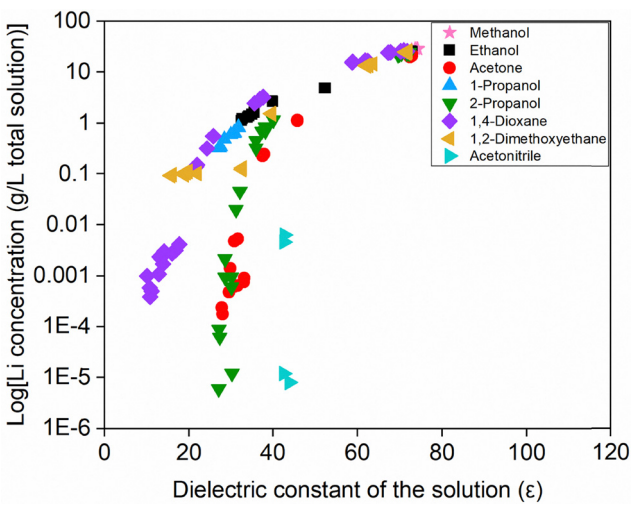

Fig. 8 Logarithm of the lithium concentration as a function of the dielectric constant of the solvent mixture.

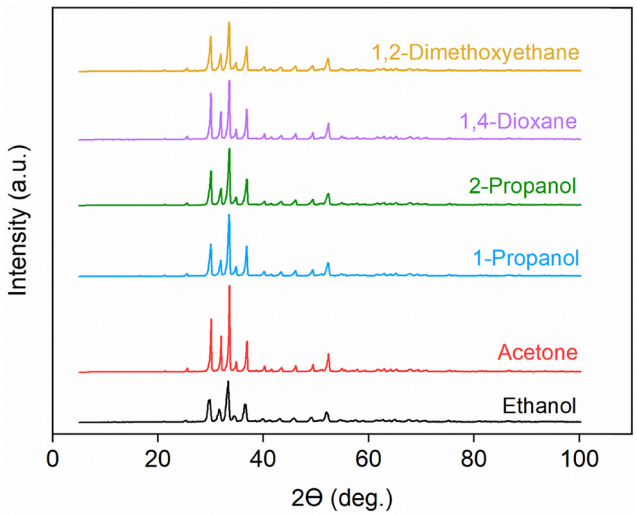

Fig. 10 XRD diffractograms confirming the presence of $LiOH{\cdot}H_2O$ using different antisolvents.

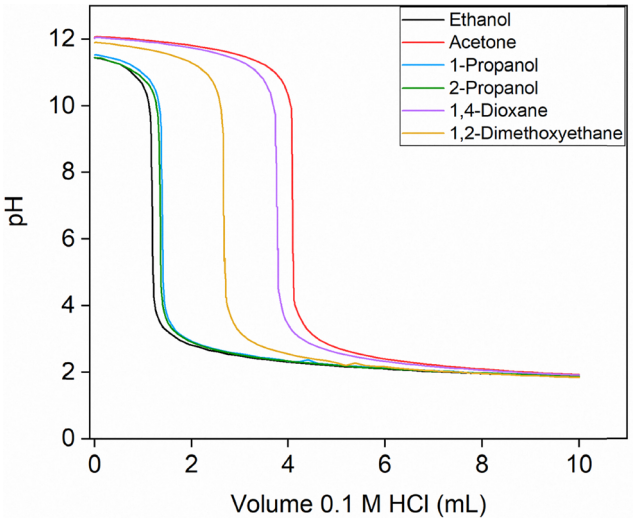

Fig. 11 Titration curves with single equivalence points, indicating no significant formation of Li_2CO_3 using different antisolvents at an 2/1 O/A ratio.

and ε_i the dielectric constant of the solvent i.[18]

$$\varepsilon = \sum_i \left(\left(\frac{x_i M_i}{\sum_j x_j M_j} \right) \varepsilon_i \right) \quad (5)$$

As shown in Fig. S15 in the SI and Fig. 8, the solubility of lithium and the log(solubility) do not align consistently with the dielectric constant of the mixture. While the dielectric constant is an important factor, it does not fully explain the solubility behavior. Other factors, such as steric hindrance, hydrogen bonding, donor ability, specific coordination interactions, or other effects also play a significant role. For example, isomers like 1-propanol and 2-propanol, still show clear differences in solubility, suggesting that molecular structure has a notable impact as well.

In Fig. 8, where the decadic logarithm of the lithium solubility is plotted, the differences between antisolvents become more pronounced at low dielectric constants. This indicates that, in this regio, the nature of the antisolvent plays a more dominant role in determining the solubility of lithium, likely due to its stronger influence on the solvation environment as water content decreases. In contrast, at higher dielectric constants, the difference between antisolvents is less, and most mixtures retain relatively high solubility. This suggests that water remains the main coordinating species in this region. As more antisolvent is added and the dielectric constant of the mixture drops, the contribution of the antisolvent to the solvation shell becomes more significant. This could explain why solubility differences between antisolvents become less pronounced at higher dielectric constants.

A clear example of this behavior is observed for 1,2-dimethoxyethane. While most solvents show a steep decline in solubility at low dielectric constant values, 1,2-dimethoxyethane exhibits a more gradual decrease. This observation supports the idea that 1,2-dimethoxyethane contributes more actively to lithium coordination at higher concentrations of antisolvent. 1,2-Dimethoxyethane can bind to lithium through two donor atoms, and may partially replace water in the coordination sphere once the water content becomes low enough. This could explain why the lithium solubility per unit mass of water increases at high 1,2-dimethoxyethane mole fractions (Table 2), even if the solubility in the total solution decreases. In other words, the lithium concentration relative to the remaining water rises because water is no longer the only effective coordinating species. For other solvents such as 2-propanol, the solubility of lithium decreases sharply at low dielectric constants, which suggests that these solvents are less effective at maintaining

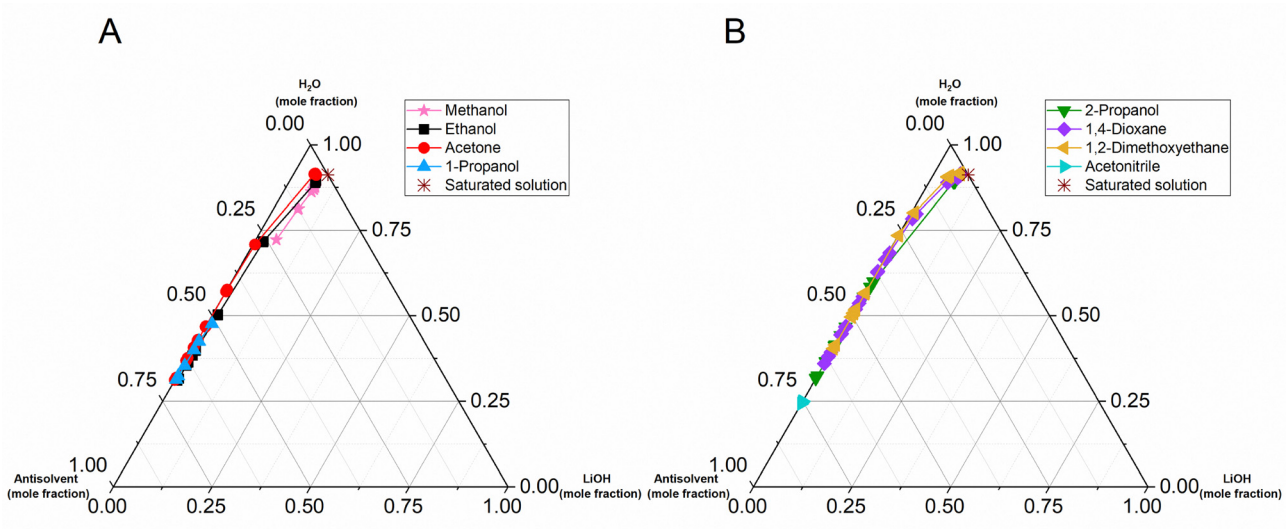

Fig. 12 Ternary phase diagrams of the LiOH–water–antisolvent systems expressed in mole fractions at 25 °C. (A) Diagrams for methanol, ethanol, acetone, and 1-propanol. (B) Diagrams for 2-propanol, 1,4-dioxane, 1,2-dimethoxyethane, and acetonitrile. The antisolvents are divided across two figures purely for visual clarity. The diagrams also indicate the composition of the saturated solution of LiOH in pure water at equilibrium.

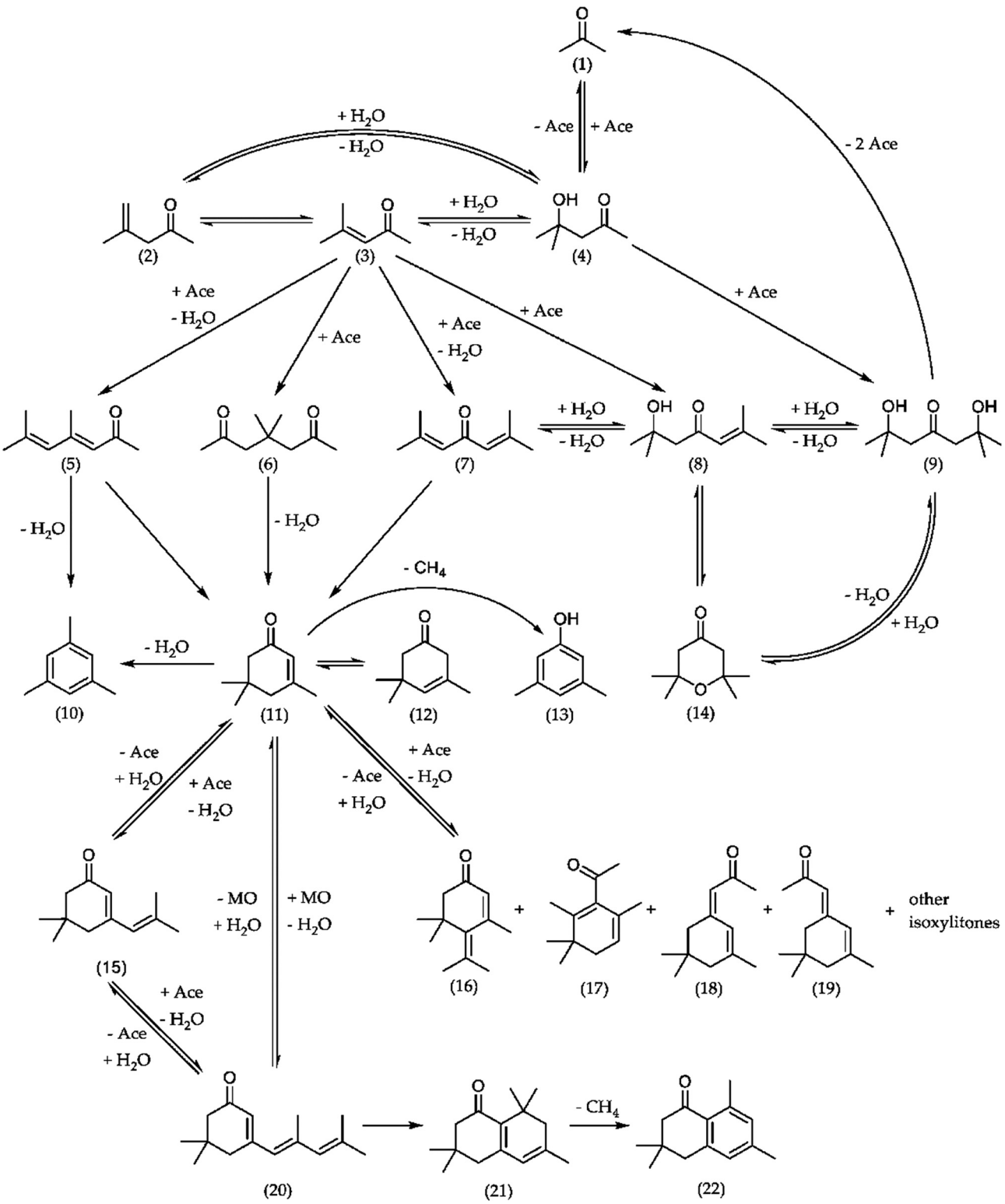

Fig. 13 Reaction scheme for the self-aldol condensation of acetone under alkaline conditions. Reproduced from Ruther *et al.*[31] under the terms of the Creative Commons Attribution (CC BY 4.0) license (https://creativecommons.org/licenses/by/4.0/).

lithium in solution under those conditions. This may indicate that water remains the dominant coordinating solvent in these mixtures, and that the added antisolvent does not provide sufficient stabilization when the water content becomes very low.

The solid phases obtained *via* the precipitation method were characterized using TGA (Fig. 9), which showed mass losses closely matching the theoretical value for $LiOH{\cdot}H_2O$. This loss, attributed to the release of water of hydration, confirms the

formation of the hydrate in all cases and is consistent with earlier observations. The TGA data shown in Fig. 9 correspond to the solids obtained at an O/A ratio of 2/1. It should be noted that acetonitrile and THF are not represented in the figure, as two immiscible liquid phases were formed at this ratio. Similarly, methanol is absent because no solid product was obtained under these conditions. XRD analysis again showed no evidence of additional phases or carbonate formation across all tested antisolvents (Fig. 10). Also acid–base titration data supported the absence of Li_2CO_3 (Fig. 11). Characterization of the solid phases from the other O/A ratios yielded consistent results across TGA, XRD, and titration analyses. The corresponding figures are provided in the SI (Fig. S16–S24).

Ternary phase diagram of the LiOH–water–antisolvent system

Given the presence of three components, LiOH, water, and an antisolvent, it is appropriate to employ a ternary phase diagram to visualize and analyze the system's equilibrium behavior. Fig. 12 shows the ternary phase diagrams of the LiOH–water–antisolvent systems at 25 °C under equilibrium conditions. In pure water, the solubility of $LiOH{\cdot}H_2O$ corresponds to a mole fraction of 0.088. The addition of antisolvents leads to a significant reduction in solubility, as reflected by the shifting of the solubility towards lower LiOH concentrations. These diagrams do not distinguish between data obtained *via* dissolution or precipitation methods, they reflect equilibrium conditions irrespective of the experimental pathway. The numerical data corresponding to these phase diagrams are provided in Table S2 in SI.

Aldol condensation of acetone

As previously mentioned, a distinct yellowish-brown to orange color was observed when acetone was used as an antisolvent. This color change is indicative of acetone undergoing self-aldol condensation in the presence of an alkaline environment (LiOH), a well-known reaction.[31] The reaction pathway for this self-aldol condensation is shown in Fig. 13, reproduced from Ruther *et al.*[31] under the terms of the Creative Commons Attribution (CC BY 4.0) license. To investigate the composition of the colored solution, ^{1}H NMR spectroscopy was used. The spectrum revealed that a complex mixture of different compounds had formed (Fig. S25 in SI). Signals in the region of 5–6 ppm are likely attributable to protons of α,β-unsaturated carbonyl compounds, while the region of 2–3 ppm is characteristic for protons in the α-position to a carbonyl group. These features are consistent with acetone undergoing aldol condensation under alkaline conditions. As the reaction time increases, more products are formed, eventually leading to phase separation, which strongly indicates the continued formation of new compounds through further condensation reactions. The formation of these by-products presents potential challenges, particularly on an industrial scale, for example, by complicating the recovery and reuse of the antisolvent.

Conclusions

The solubility of lithium hydroxide monohydrate was systematically studied in pure water and in various mixtures of different antisolvents using the isothermal dissolution method and the precipitation method. Solid–liquid equilibrium was reached fast across all systems, and a 24-hour equilibration period was selected. In pure water at 25 °C, the solubility was determined to be 12.53 ± 0.09 g of LiOH per 100 g of H_2O, which was in close agreement with literature values. Characterization of the solid phases by TGA, XRD, and acid–base titration confirmed the formation of $LiOH{\cdot}H_2O$ with no significant presence of Li_2CO_3 or anhydrous LiOH.

$LiOH{\cdot}H_2O$ solubility decreased with increasing antisolvent content although the behavior varied per solvent. $LiOH{\cdot}H_2O$ had a high solubility in methanol and ethanol, while solvents such as 1,4-dioxane and 1,2-dimethoxyethane effectively reduced solubility but raised concerns about sustainability and safety. Acetone showed evidence of self-aldol condensation, limiting its suitability. 2-Propanol was selected as the most suitable antisolvent due to its effective reduction of LiOH solubility, miscibility with water, chemical stability, favorable safety, cost, distillation feasibility after use and environmental impact. The agreement between the dissolution and precipitation methods confirmed that solid–liquid equilibrium was consistently achieved under the applied experimental conditions.

Author contributions

Lien Lemmens: conceptualization, investigation, experimental work and writing – original draft. Xavi Vanwezer: experimental work. Stijn Raiguel: conceptualization, writing – review & editing. Rayco Lommelen: conceptualization, writing – review & editing. Kerstin Forsberg: conceptualization, writing – review & editing. Tom Van Gerven: conceptualization, supervision, writing – review & editing. Koen Binnemans: conceptualization, supervision, writing – review & editing, funding acquisition.

Conflicts of interest

There are no conflicts to declare.

Data availability

The data supporting this article have been included as part of the Supplementary Information (SI). The SI includes TGA results, powder XRD analysis results, titration graphs, lithium concentrations as a function of the mole fraction of antisolvent for each antisolvent separately, lithium concentrations as a function of the dielectric constant of the solvent mixture, data for ternary phase diagrams, and the ^{1}H NMR spectrum related to the acetone aldol condensation. See DOI: https://doi.org/10.1039/d5cp04491j.

Acknowledgements

This research was supported by the European Union's Framework Programme for Research and Innovation Horizon Europe *via* project LITHOS [grant number 101138112]. The authors acknowledge Dr. Nandi Snehashis and Dr. Nitin Pawar (KTH, Sweden) for their assistance in the laboratory and for the valuable discussions conducted in Sweden.

References

1 N. Peeters, S. Riaño and K. Binnemans, Conversion of Lithium Chloride into Lithium Hydroxide Using a Two-Step Solvent Extraction Process in an Agitated Kühni Column, *J. Sustainable Metall.*, 2024, **10**, 637–645, DOI: 10.1007/s40831-024-00815-4.

2 V. T. Nguyen, C. Deferm, W. Caytan, S. Riaño, P. T. Jones and K. Binnemans, Conversion of Lithium Chloride into Lithium Hydroxide by Solvent Extraction, *J. Sustainable Metall.*, 2023, **9**, 107–122, DOI: 10.1007/s40831-022-00629-2.

3 A. K. Koech, G. Mwandila, F. Mulolani and P. Mwaanga, Lithium-ion battery fundamentals and exploration of cathode materials: A review, *S. Afr. J. Chem. Eng.*, 2024, **50**, 321–339, DOI: 10.1016/j.sajce.2024.09.008.

4 M. Ahmadi, A. Ghaemi and M. Qasemnazhand, Lithium hydroxide as a high capacity adsorbent for CO_2 capture: experimental, modeling and DFT simulation, *Sci. Rep.*, 2023, **13**, 7150, DOI: 10.1038/s41598-023-34360-z.

5 J. M. Paulsen, H. Park and Y. H. Kwon, Process of making cathode material containing Ni-based lithium transition metal oxide, *US Pat.*, US7943111B2, 2011.

6 P. Meshram, B. D. Pandey and T. R. Mankhand, Extraction of lithium from primary and secondary sources by pretreatment, leaching and separation: A comprehensive review, *Hydrometallurgy*, 2014, **150**, 192–208, DOI: 10.1016/j.hydromet.2014.10.012.

7 J. M. Dahlkamp, C. Quintero, A. Videla and R. Rojas, Production processes for LiOH – A review, *Hydrometallurgy*, 2024, **223**, 106217, DOI: 10.1016/j.hydromet.2023.106217.

8 K. H. Choi and G. Azimi, Crystallization of nickel sulfate and its purification process: towards efficient production of nickel-rich cathode materials for lithium-ion batteries, *RSC Adv.*, 2023, **13**, 28501–28512, DOI: 10.1039/D3RA04280D.

9 H. S. Demirel, M. Svärd, D. Uysal, Ö. M. Doğan, B. Z. Uysal and K. Forsberg, Antisolvent crystallization of battery grade nickel sulphate hydrate in the processing of lateritic ores, *Sep. Purif. Technol.*, 2022, **286**, 120473, DOI: 10.1016/j.seppur.2022.120473.

10 J. M. Schall and A. S. Myerson, in Handbook of Industrial Crystallization, Cambridge University Press, 3rd edn, 2019, *Solutions and Solution Properties*, pp. 1–31.

11 M. E. Taboada, H. R. Galleguillos, T. A. Graber and J. Álvarez-Benedí, Density, viscosity, refractive index and electrical conductivity of saturated solutions of the lithium hydroxide + ethanol + water system at 298.15 K, and thermodynamic description of the solid-liquid equilibrium, *Fluid Phase Equilib.*, 2005, **235**, 104–111, DOI: 10.1016/j.fluid.2005.05.022.

12 A. Chagnes and K. Forsberg, Raw Material Supply for Lithium-Ion Batteries in the Circular Economy, *Metals*, 2023, **13**(9), 1590, DOI: 10.3390/met13091590.

13 M. E. Taboada, T. A. Graber, L. A. Cisternas, Y. S. Cheng and K. M. Ng, Process design for drowning-out crystallization of lithium hydroxide monohydrate, *Chem. Eng. Res. Des.*, 2007, **85**, 1325–1330, DOI: 10.1205/cherd06251.

14 T. A. Graber, J. W. Morales, P. A. Robles, H. R. Galleguillos and M. E. Taboada, Behavior of $LiOH{\cdot}H_2O$ crystals obtained by evaporation and by drowning out, *Cryst. Res. Technol.*, 2008, **43**, 616–625, DOI: 10.1002/crat.200711110.

15 L. V. Gurvich, G. A. Bergman, L. N. Gorokhov, V. S. Iorish, V. Y. Leonidov and V. S. Yungman, Thermodynamic properties of alkali metal hydroxides. Part 1. Lithium and sodium hydroxides, *J. Phys. Chem. Ref. Data*, 1996, **25**, 1211–1276, DOI: 10.1063/1.555982.

16 R. González, Y. Barrueto and Y. P. Jiménez, Thermodynamic Modeling of the Drowning-Out Crystallization Process for LiOH and $CHLiO_2$, *Metals*, 2024, **14**(1), 78, DOI: 10.3390/met14010078.

17 Y. Deng, T. Howes and J. Vaughan, Membrane Percrystallization for Production of Lithium Salt and Basic Compounds, *JOM*, 2025, **77**, 8272–8284, DOI: 10.1007/s11837-025-07464-2.

18 C. Ma, M. Mohamoud, T. Punt, J. Li, M. Svärd and K. Forsberg, Crystallization of Cathode Active Material Precursors from Tartaric Acid Solution, *ChemSusChem*, 2025, **18**, e202401523, DOI: 10.1002/cssc.202401523.

19 C. Ma, J. D. Gamarra, R. Younesi, K. Forsberg and M. Svärd, Antisolvent crystallization from deep eutectic solvent leachates of $LiNi_{1/3}Mn_{1/3}Co_{1/3}O_2$ for recycling and direct synthesis of battery cathodes, *Resour., Conserv. Recycl.*, 2023, **198**, 107210, DOI: 10.1016/j.resconrec.2023.107210.

20 E. M. Peters, M. Svärd and K. Forsberg, Phase equilibria of ammonium scandium fluoride phases in aqueous alcohol mixtures for metal recovery by anti-solvent crystallization, *Sep. Purif. Technol.*, 2020, **252**, 117449, DOI: 10.1016/j.seppur.2020.117449.

21 Z. Li and G. P. Demopoulos, Solubility of $CaSO_4$ phases in aqueous HCl + $CaCl_2$ solutions from 283 K to 353 K, *J. Chem. Eng. Data*, 2005, **50**, 1971–1982, DOI: 10.1021/je050217e.

22 W. F. Linke and A. Seidell, *Solubilities Inorganic and Metal-Organic Compounds*, American Chemical Society, Washington, DC, 4th edn, vol. 2, 1958.

23 D. R. Lide, *CRC Handbook of Chemistry and Physics*, CRC Press, Boca Raton, FL, 85th edn, 2005.

24 S. Shakibania, L. Sundqvist-Öqvist, J. Rosenkranz and Y. Ghorbani, Application of Anti-Solvent Crystallization for High-Purity Potash Production from K-Feldspar Leaching Solution, *Processes*, 2024, **12**(7), 1385, DOI: 10.3390/pr12071385.

25 C. M. Alder, J. D. Hayler, R. K. Henderson, A. M. Redman, L. Shukla, L. E. Shuster and H. F. Sneddon, Updating and further expanding GSK's solvent sustainability guide, *Green Chem.*, 2016, **18**, 3879–3890, DOI: 10.1039/C6GC00611F.

26 ed W. M. Haynes, D. R. Lide and T. J. Bruno, *CRC Handbook of Chemistry and Physics*, CRC Press, Taylor & Francis Group, 97th edn, 2016.
27 F. M. Vieira, F. S. Buarque, P. G. C. Gomes, R. L. Souza, C. M. F. Soares, M. H. A. Santana and Á. S. Lima, Partition of humic acids using alkaline aqueous two-phase systems constituted of alcohol and hydroxides, *J. Chem. Technol. Biotechnol.*, 2024, **99**, 1012–1021, DOI: 10.1002/jctb.7610.
28 L. H. Horsley, Azeotropic Data. *Advances in Chemistry Series*, American Chemical Society, Washington DC, 1952, vol. 6.
29 J. Sussens, J. Chivavava and A. E. Lewis, The recovery of yttrium sulfate through antisolvent crystallization using alcohols, *Sep. Purif. Technol.*, 2024, **346**, 127459, DOI: 10.1016/j.seppur.2024.127459.
30 F. Cataldo, A revision of the Gutmann donor numbers of a series of phosphoramides including TEPA, *Eur. Chem. Bull.*, 2015, **4**, 92–97, DOI: 10.17628/ECB.2015.4.92-97.
31 T. Ruther, M.-A. Müller, W. Bonrath and M. Eisenacher, The Production of Isophorone, *Encyclopedia*, 2023, **3**, 224–244, DOI: 10.3390/encyclopedia3010015.